

**Numerical Simulation of Nano Scanning in Tapping
Mode AFM under Q control**

by

Aydin Varol

**A Thesis Submitted to the
Graduate School of Engineering
in Partial Fulfillment of the Requirements for
the Degree of**

**Master of Science
in
Mechanical Engineering**

Koc University

September 2007

Koc University
Graduate School of Sciences and Engineering

This is to certify that I have examined this copy of a master's thesis by

Aydin Varol

and have found that it is complete and satisfactory in all respects,
and that any and all revisions required by the final
examining committee have been made.

Committee Members:

Cagatay Basdogan, Ph. D. (Advisor)

Erdem Alaca, Ph. D.

Alper Kiraz, Ph. D.

Date:

ABSTRACT

In this thesis, we investigate nano scanning in tapping mode atomic force microscopy (AFM) under quality (Q) control via numerical simulations performed in SIMULINK. We focus on the simulation of whole scan process rather than the interactions between the AFM probe and the surface only. This enables us to quantify the scan performance under Q control for different scan variables and settings. We first demonstrate the trade-off in setting the effective Q factor (Q_{eff}) of a cantilever probe in standard Q control. Low values of Q_{eff} causes an increase in tapping forces while higher ones limit the maximum achievable scan speed due to the slow response of the cantilever to the rapid changes in surface profile. We then show that it is possible to achieve higher scan speeds without causing an increase in the tapping forces using adaptive Q control (AQC), in which the Q factor of cantilever is changed instantaneously depending on the magnitude of error signal in oscillation amplitude. The scan performance of AQC is quantitatively compared to that of standard Q control using iso-error curves obtained through numerical simulations first and then validated through scan experiments performed in a physical set-up.

ÖZET

Bu tezde, kalite faktörü (Q) kontrollü altında çalışan bir atomik kuvvet mikroskopunun (AKM) nano boyutlardaki bir yüzeyi taramasını SIMULINK simülasyonları ile inceledik. Sadece tarama probunun dinamiğine değil, tarama işleminin bütünün simülasyonuna odaklandık. Bu sayede, Q kontrollü taramanın, değişik tarama değişkenleri ve ayarları için performansını sayısal olarak inceledik. İlk önce, probun etkin Q faktörünü ayarlamadaki ödünleşmeyi gösterdik. Düşük Q faktörü, prob ucu ile taranan yüzey arasındaki etkileşim kuvvetlerini artırırken, yüksek değerler tarama hızını sınırlandırmaktadır. Daha sonra, hata sinyalinin genliğine göre probun Q faktörünü anlık olarak değiştiren uyarlanabilir (adaptif) Q kontrolü kullanarak etkileşim kuvvetlerini artırmadan da daha yüksek tarama hızlarına ulaşmanın mümkün olduğunu gösterdik. Adaptif Q kontrolü sayısal olarak hesaplanan eş hata çizgileri kullanılarak standart Q kontrolü ile karşılaştırıldı ve sonuçlar deney düzeneğinde yapılan tarama deneyleriyle desteklendi.

ACKNOWLEDGEMENTS

I wish to express my sincere gratitude to my thesis supervisor Assistant Prof. Çağatay Başdoğan for his support, valuable criticism, and endless patience throughout my study. I would like to thank Assistant Prof. Erdem Alaca, Assistant Prof. Alper Kiraz for their valuable comments and time in reviewing this thesis as my committee members. I would also like to thank Dr. Hakan Urey for giving me the opportunity working in his laboratory and using their equipments. Thanks to, my precious friend İhsan Günev for his assistance during building up my experimental set-up and his friendship both during and after the lab hours and Sertac Karaman for his great knowledge on control theory and for his research on adaptive Q control. Also I would like to thank Bilal Örün for his help during the lab hours. I would like to thank to my close friend Uğur Kaplan for his encouragement and support. I was fortunate to have such great friends close to me during my graduate education; Ali Alagöz, Emrah Ahi, Hüseyin Alptekin and Lütfi Mert Sedef my homemates, Mustafa Kaymakci, Onur Demir, Gokhan Yıldız, Galip Tarkan Güçlü, and Murat Senan my officemates. Thanks to Google Inc. for leading me to quite most of the information I am searching for, and to all of the graduate students working in KU Labs for allowing me to dig and use their material stock. Finally, I would like to express my special thanks to my family for their endless love and patience throughout my study.

TABLE OF CONTENTS

List of Tables	viii
List of Figures	ix
Chapter 1: Introduction	1
Chapter 2: Setup	7
2.1 Scanning System	4
2.1.1 Signal Processing Circuit	11
Chapter 3: Cantilever Dynamics	16
3.1 Cantilver Model	16
3.2 Force Model	18
3.2.1 Non-contact Forces	19
3.2.1 Contact Forces	19
Chapter 4: Simulink Model	21
4.1 Models of the Physical Components in the Setup	21
4.1.1 Vibrometer	21
4.1.2 RMS Converter	22
4.1.3 PI Scan Controller	22
4.1.4 XYZ Stage	22
4.1.5 Adaptive Q Controller	23

4.2	Models for Input/Output Operations	23
4.2.1	Input Profile	23
4.2.2	Output Profile	24
Chapter 5:	Scanning Simulations and Experiments	25
Chapter 6:	Discussion and Conclusion	43
Bibliography		46
Vita		49

LIST OF TABLES

Table 2.1: The dynamical characteristics of the probe.	15
--	----

LIST OF FIGURES

Figure 1.1: A schematic representation of driven cantilever probe.	3
Figure 2.1: The components of the developed AFM set-up.	8
Figure 2.2:	9
a) The image of the probe used in the set-up under optical microscope.	
b) The probe is supplied by the manufacturer as glued and wire bonded on a chip.	
Figure 2.3: The signal processing circuit.	13
Figure 3.1: The frequency response of the cantilever	18
Figure 4.1: .SIMULINK model of our experimental scanning set-up.	24
Figure 5.1:	27
a) Apparent height of a 10 nm sample	
b) Oscillation amplitude versus mean tip-sample distance	
Figure 5.2:	30
a) Maximum tapping forces.	
b) The rate of change in tapping.	
Figure 5.3: Scanning a downward step.	32
Figure 5.4: Scan Error Definition.	34
Figure 5.5: Iso-error curves for the scan results of a 100 nm step	36
Figure 5.6: The error saturations	38
Figure 5.7: Results of the experimental and numerical scans	40

Figure 5.8: The error signal during the scanning	41
Figure 5.9: Comparison of standard Q control and AQC	42

Chapter 1

INTRODUCTION

In tapping-mode dynamic force microscopy (DFM), a cantilever probe, oscillating in free-air around resonant frequency with an amplitude of A_0 , is used to scan a sample surface [1]. When the tip of the probe taps the sample surface lightly for a very short period of time, the oscillation amplitude is reduced to $A < A_0$. In amplitude modulation scheme, a scan controller moves the sample or the probe in vertical direction (i.e. z-direction) such that the oscillation amplitude during tapping stays constant at set amplitude A_{set} . These up and down movements in vertical direction are recorded during scanning to construct the surface profile of the sample.

During tapping-mode scanning, the interaction forces between the probe tip and the sample surface are highly nonlinear and the response of the cantilever probe to these forces is primarily governed by its quality factor, $Q = \Delta\omega/\omega_n$, where ω_n is the n^{th} resonance frequency of the cantilever and $\Delta\omega$ is the width of the resonance curve for which the energy is greater than the half of its peak. The Q factor of a cantilever probe indicates its energy dissipation capacity or damping present in the system. A probe with low Q factor dumps its

energy faster, resulting in lower-amplitude steady-state oscillations and a rounded resonance curve. On the other hand, a probe with high Q factor (one with low damping) oscillates more and its resonance curve shows a sharp peak.

The Q factor of a cantilever probe can be set to a value using an additional feedback circuit. By applying an appropriate force to the oscillating cantilever, its motion can be regulated in such a way that the modified response of the system shows an increased or decreased Q factor. This approach is known as “Q control” and has been suggested as an effective method in DFM [2]. In Figure 1.1, a schematic illustration of a Q controlled cantilever probe with the electronics required to modify its Q factor is presented. Typically, a phase shifter and an amplifier with a gain G are used in the feedback circuit in order to control the Q factor of an oscillating cantilever. First, the displacement signal of an oscillating probe is measured using a photo-detector, shifted in phase using the phase shifter, and then scaled by the gain G , and finally used as the velocity signal in the feedback loop. This velocity signal is added to (or subtracted from) the driving signal to decrease (or to increase) the effective damping of the cantilever. We hereafter will call this approach where the gain G is set to a constant value before the scan process as standard Q control in the text.

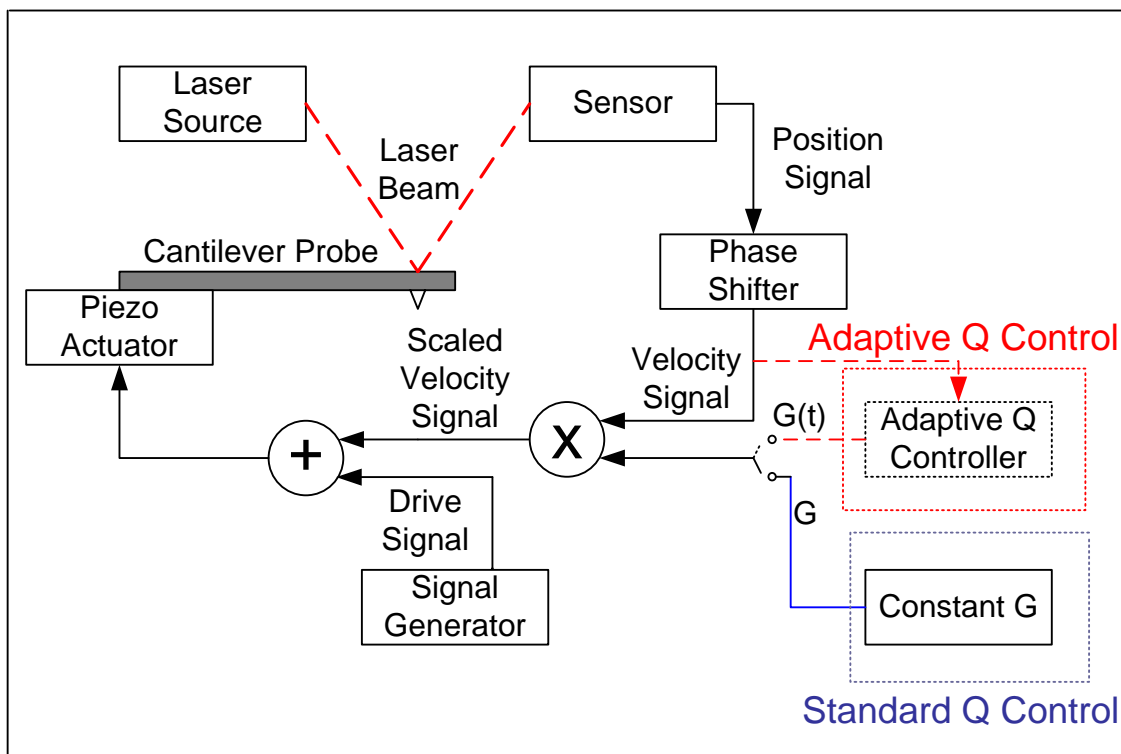


Figure 1.1: A schematic representation of driven cantilever probe in tapping mode scanning under standard (blue solid line) and adaptive (red dashed line) Q control. The gain G is constant in standard Q control whereas it is adjusted in real-time based on the surface profile in adaptive Q control.

Studies have shown that the image resolution improves with Q control, but the mechanism for this is still not well-understood [3-5]. Rodriguez and Garcia developed an analytical solution for an oscillating probe under Q control [6]. Their simulations suggested that the slope of the amplitude-distance curves is substantially larger implying a higher sensitivity

to tip-surface variations, which results in better image quality. However, numerical simulations performed later by Kokavecz et al. yielded that the slope of the amplitude versus distance curves is not increased for stiff samples and hence they concluded that the maximal probe sensitivity cannot be increased with Q control [7]. Holscher et al. performed numerical simulations and found that an increased Q factor prevents the oscillating cantilever to jump into a repulsive imaging regime during tip-sample approach, which often occurs in tapping mode imaging without Q control [8]. They concluded that restriction of the maximal tip-sample force to specific parts of the attractive regime in Q control is the main reason for the enhanced imaging quality. Hence, it can be argued that Q control keeps the probe in the attractive regime longer and as a result, the magnitude of the average tapping forces is reduced. In fact, Jäggi et al. experimentally determined that the average tip-sample forces are reduced by Q control [9].

While Q control improves the image quality, there is a trade-off in setting the Q factor of a scanning probe, which has not been investigated in detail. For example, increasing the Q factor of the probe enables scanning in liquid where the native Q factor is reduced significantly due to the environmental damping. By implementing the Q control, the Q factor can be increased up to three orders of magnitude. Since the interaction forces between the probe tip and the sample are reduced by using a cantilever probe having a high Q factor, damaging the sample (i.e. soft biological samples) is also prevented [10]. On the

other hand, the mechanical sensing bandwidth of the probe is inversely proportional to its quality factor, which limits the maximum achievable scan speed (i.e. the maximum speed that the probe can trace the sample surface with a reasonable amount of positional error in scan profile). Sulchek et al. showed that the sensing bandwidth of a scanning probe and scan speed can be improved significantly by actively lowering the Q factor of the probe when scanning stiff surfaces in air [11, 12].

Hence, the effective Q factor (Q_{eff}) of the probe is set to a value that is lower or higher than its native one before scanning in standard Q control and achieving higher scan speeds with reduced tapping forces is not possible. Gunev et al suggested that these two benefits can be realized simultaneously using AQC [13]. They developed a signal processing circuit that adjusts the gain G on the fly during scanning depending on the error in amplitude signal. If there is a tendency towards saturation in error (as it typically occurs in scanning steep downward steps), the controller increases the Q factor of the probe rapidly to avoid the problem.

In this study, we investigated the trade-off in Q control through numerical simulations performed in SIMULINK. In particular, we investigated the effect of scan speed and A_{set}/A_0 on scan performance. Moreover, we showed that AQC solves the trade-off problem and expands the allowable workspace. In most of the earlier numerical studies, the

differential equation governing the dynamics of the cantilever probe has been investigated only, but the transient effects during scanning have been neglected (i.e. only the steady state solution of cantilever oscillations is considered). These studies have primarily investigated the effect of various parameters and tip-sample forces on cantilever dynamics. Moreover, the parameters of the cantilever model are not based on the experimental measurements and selected somehow arbitrarily to meet the simulation requirements. We categorize this type of numerical studies as “cantilever” simulations to differentiate it from our work of “scanning” simulations. To our knowledge, there are only a few studies focusing on the end-to-end simulation of whole scanning process [14]. Our simulations not only integrate the model of cantilever, but also the models of other components of the scanning system such as the scan controller, measurement devices, and DAQ sampling unit. This is achieved using SIMULINK, which provides a flexible computing environment for supporting linear and nonlinear systems, modeled in continuous time, sampled time, or a hybrid of the two. The detailed SIMULINK models of the components used in our scanning system are discussed in the upcoming sections. Moreover, our numerical simulations performed in SIMULINK are supported by the experiments conducted using a homemade AFM set-up.

Chapter 2

SETUP

2.1 Scanning System

We have developed a new AFM set-up operating in tapping mode to conduct scanning experiments with Q control. The components of the set-up are shown in Figure 2.1. All movements of the sample relative to the scanning probe is controlled using a XYZ nano-stage (PI Inc, Germany, Model No: P-517.3CD) combined with a 3 channel digital controller unit (E-710.P3D). The nano-stage has a travel range of 100 x 100 x 20 μm and equipped with integrated capacitive sensors for precise positioning (nominal resolution is 0.1 nm). The digital controller of the stage is connected to a digital data acquisition (DAQ) card (PCI-DIO-96, National Instruments Inc.) via parallel input/output port running a servo loop at 5ms/cycle. The usage of a digital nano-stage brings high accuracy positioning with velocity controlled motion, noiseless operation, and accurate measurement of XYZ position. Moreover, it significantly reduces the non-linearity and creep typically observed in open-loop scanning systems utilizing a piezo tube (PZT) as the positioning device.

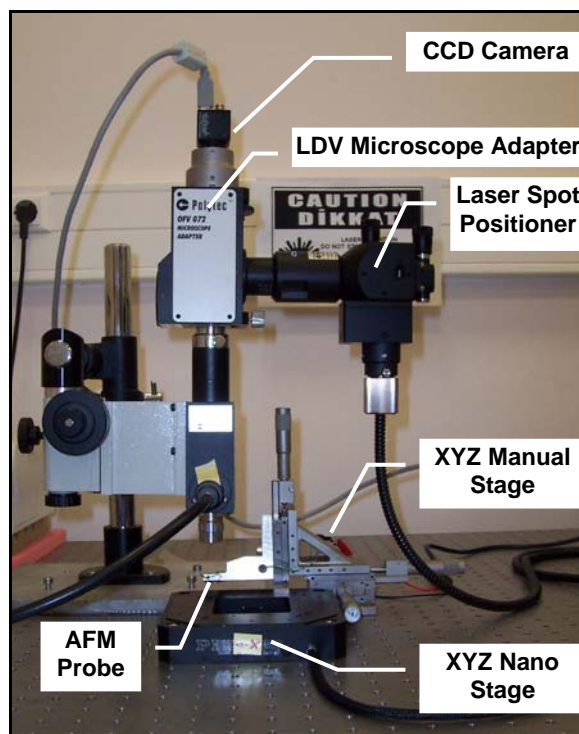


Figure 2.1: The components of the developed AFM set-up.

A commercially available self-actuated AFM probe (DMASP, Veeco Probes Inc., Santa Barbara, CA) is used for scanning. The probe contains a ZnO stack (consisting of $0.25\mu\text{m}$ Ti/Au, $3.5\mu\text{m}$ ZnO, and $0.25\mu\text{m}$ Ti/Au) at its base [15]. This stack, along with the silicon cantilever, acts as a bimorph actuator to oscillate the probe up and down (Figure 2.2.a). When voltage signals are applied to the pads at the fixed end of the cantilever, the ZnO layer expands or contracts according to the piezoelectric phenomena causing the bimorph probe tip to oscillate. In this way, the cantilever can be resonated by applying

voltage signals at a desired frequency. The probe which is already glued and wire bonded on a chip by the manufacturer (Figure 2.2.b) is mounted on a manual XYZ stage (462 Series, Newport Inc., Germany) to bring it sufficiently close to the sample surface.

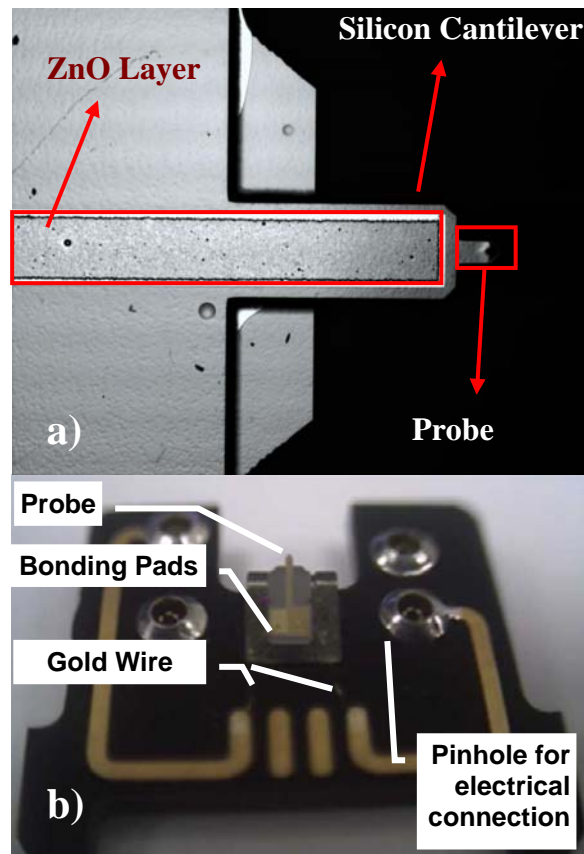


Figure 2.2: a) The image of the probe used in the set-up under optical microscope (tip side is up). b) The probe is supplied by the manufacturer as glued and wire bonded on a chip.

An electrical signal for the actuation of the probe is provided by a signal generator (Agilent Technologies Inc, Model No: 33220A). A Laser Doppler Vibrometer, LDV, (Polytec GmbH, Germany.) is used for measuring the vertical vibrations of the probe. The LDV having a bandwidth of 1.5GHz, measures the out of plane velocity of a point on the probe by collecting and processing the back-scattered laser light. It is composed of a controller (OFV-5000) and a fiber interferometer (OFV-551). The sensor head of OFV-551 delivers a He-Ne red laser beam ($\lambda = 633 \text{ nm}$) to a measurement point on the probe and collects the reflected light. Using an optical microscope (VM-1V, Meiji Techno Co., Ltd, Japan) with 5X lens, the laser beam is focused down to a spot size of $\sim 2 \text{ }\mu\text{m}$. The controller OFV-5000 processes the data collected from OFV-551 using a wide bandwidth velocity decoder (VD-02) having a resolution of $0.15 \text{ }\mu\text{m/s}$. The measurement data is acquired from the LDV controller (OFV-5000) in scaleable units of mm/s/V. In addition, Polytec OFV-71 and OFV-72 units are mounted between the microscope and the CCD camera (Flea, Point Grey Research Inc., Vancouver, Canada) to integrate the microscope system with the OFV-551. OFV-71 contains movable mirrors to deflect the laser beam so that one can manually position the laser spot in the area of view (AOV) of the microscope.

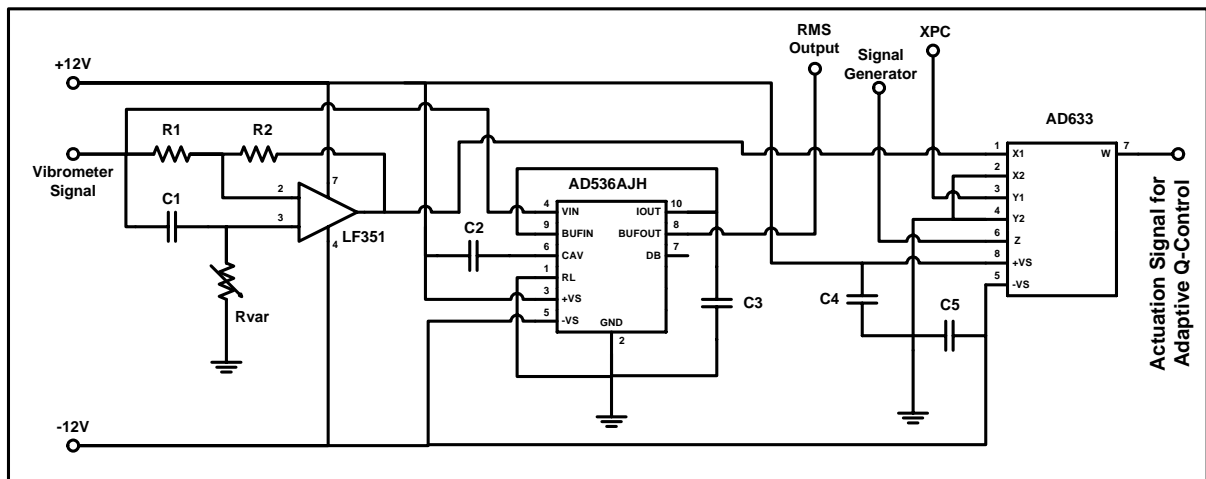


Figure 2.3: The signal processing circuit.

2.1.1 Signal Processing Circuit

An analog signal processing circuit (Figure 2.3) consisting of a) a root mean square (RMS) converter, b) a variable phase-shifter, and c) a voltage-multiplier is built and integrated into the AFM system to adaptively modify the Q-factor of the probe on the fly during scanning.

a) RMS converter: In order to obtain the vibration amplitude of the probe from the measured velocity signal in real-time, an analog RMS converter is used. Since, an AFM probe is typically vibrated at or close to its resonant frequencies for better scanning results, the acquisition of complete sinusoidal velocity signal requires high-speed sampling. This requirement is eliminated by using an integrated circuit (AD536AJH, Analog Devices, Norwood, MA) which computes the RMS value of the vibrometer output at update rates

higher than the sensing bandwidth of the probe (see Figure 2.3). The capacitor C2 shown in adjusts the width of the running RMS window. Choosing a low value for C2 improves the bandwidth of the RMS converter but increases the ripple in the output. The capacitor C3 acts like a single-pole post-filter and increases the quality of the output signal and the bandwidth of the converter.

b) Phase-shifter: An analog phase-shifter is integrated into the signal processing circuit to eliminate the intrinsic time delay in the LDV and hence to obtain a true velocity signal. Although the LDV used in our set-up is equipped with a velocity decoder and directly measures the vibration velocity of the probe, we observed a constant time delay ($\sim 4\mu\text{s}$) in the measurement signal, which causes an additional phase lag between the actuation and output signals. Further experiments and the discussions with the manufacturer of the LDV confirmed that the source of this delay is the time spent by the LDV controller for the digital signal processing. To eliminate the phase lag due to this constant time delay, the resistance in the phase shifter (R_{var} in Figure 2.3) is adjusted in advance such that the output comes from the phase shifter is always in phase with the true velocity signal.

c) Voltage-multiplier: In order to multiply the phase-corrected velocity signal by the variable gain $G(t)$ as discussed earlier, an analog voltage multiplier (AD633, Analog Devices, Norwood, MA) is integrated into the signal processing circuit. This unit enables us to modify the Q-factor of the probe on the fly during scanning when necessary. The transfer function of the AD633 chip, supplied by the manufacturer, is

$W(t)=[V(t)*G(t)]/10+P(t)$, where in our case, $P(t)$ is the periodic actuation signal coming from the signal generator at or close to the resonant frequency of the probe, $V(t)$ is the phase-corrected velocity signal, $G(t)$ is the variable feedback gain adjusted by the adaptive Q-controller running on an xPC Target (The MathWorks, Inc.), and $W(t)$ is the actuation signal sent to the probe. Using AD633, the measurement signal is first multiplied by $G(t)$ and then added to the actuation signal to modify the Q-factor of the probe.

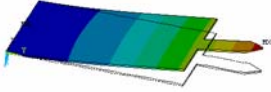
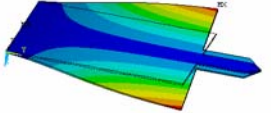

The xPC Target runs a real-time controller which takes the RMS of the velocity signal as input and outputs the feedback gain $G(t)$. The software for the controller is developed in Matlab/Simulink (The MathWorks, Inc.) and then converted to C code using the Real-Time Workshop (The MathWorks, Inc.) and compiled by Microsoft Visual Studio C++. The computer running the xPC Target is a high-performance PC equipped with a DAQ card (PCI-6025E, National Instruments Inc.) which enables the data communication between the xPC Target and the signal processing circuit.

In order to scan a sample using the developed AFM system, the velocity of the probe tip is measured as a continuous signal using the LDV and then this signal is converted to an RMS signal and sampled by a DAQ card (PCI-6034E, National Instruments Inc.) into a computer. The oscillation amplitude of the probe A is calculated from the RMS signal and then compared with the desired oscillation amplitude A_{set} . A scan-controller (PI-controller) developed in LabVIEW (National Instruments Inc.) keeps the vibration amplitude of the

probe constant during raster scanning by moving the nano stage up and down along the Z-axis based on the error signal ($A_{set} - A$).

The native Q-factors of the probe for the first three vibration modes of the cantilever are calculated from the amplitude versus frequency response curves by measuring the full width at half maximum (FWHM) bandwidth. The Q-factor of the probe at the resonance frequency ω_R is calculated from the ratio of ω_R/FWHM (see Table 2.1). Alternatively, the Q-factor of the probe can be calculated using the amplitude modulation method [16]. The mode shape of the probe at the second resonance frequency is torsional; hence it cannot be used for scanning in tapping-mode AFM. The first and third modes are flexural and the third one is preferred over the first one due to its smaller time constant $T = Q/\omega_R$, where $1/T$ is defined as the sensing bandwidth of the probe. Cantilevers with higher bandwidth responds faster to the perturbations and enable scanning at higher speeds. As it can be seen from the table, the bandwidth of the third mode is higher than that of the first mode.

Table 2.1: The dynamical characteristics of the probe for the first three resonance modes.

Mode	Mode Shape	Resonance Frequency (Hz)	Quality Factor	Bandwidth (Hz)
1 st		48.600	129	376
2 nd		180.000	-	-
3 rd		210.000	311	675

Chapter 3

CANTILEVER DYNAMICS

3.1 Cantilever Model

A damped mass-spring system is used to model the dynamical behavior of the cantilever. This model is typically utilized by the earlier AFM studies and it is a reasonable approximation of the oscillating cantilever [10, 17, 18]. It is assumed that the cantilever is externally driven by a sinusoidal force F_{drive} at its resonance frequency ω . In addition to the driving force, the oscillations of the cantilever are also influenced by the interaction forces between the cantilever tip and sample surface, F_{ts} . This force is a function of tip-sample separation distance h . The dynamics of the cantilever probe can be written as a second-order differential equation in the form of

$$m\ddot{z} + b\dot{z} + kz = F_{\text{drive}} + F_{\text{ts}}(h) \quad (3.1)$$

where, k and m are the effective spring constant and mass of the cantilever respectively. In addition, a damper with a coefficient b is added to the model to simulate structural damping and damping due to air. The damper applies a resistance to the oscillations proportional to

the vibration velocity of the cantilever and causes energy dissipation. Expressing the above equation in terms of measurable quantities, we have the following equation

$$m\ddot{z} + \frac{m\omega}{Q}\dot{z} + kz = F_0 \cos(\omega t) + F_{ts}(h) \quad (3.2)$$

where, the magnitude of the external driving force is F_0 . The Q factor of the cantilever is inversely proportional with the damping coefficient b . For a system with high Q factor (low damping), the resonance frequency of the system is approximately equal to its natural frequency $\omega_n \approx \omega = \sqrt{k/m}$. The Q factor and the resonance frequency ω of the cantilever can be determined experimentally by examining its frequency response. The frequency response of the cantilever used in our experimental set-up is plotted for different gains G and matched to the one used in our numerical simulations (Figure 3.1). From the plots, the resonance frequency of the cantilever (260 kHz) is determined as the frequency at which the oscillation amplitude reaches to maximum and the Q factor of the probe ($Q_{\text{native}} = 311$) is determined by measuring the frequency range $\Delta\omega$ where the energy of the oscillations is greater than half of the maximum energy at the resonance frequency. The value of the spring constant used in the numerical model is obtained from the catalog of the manufacturer of the cantilever (the nominal value is reported as 3 N/m at the operating frequency).

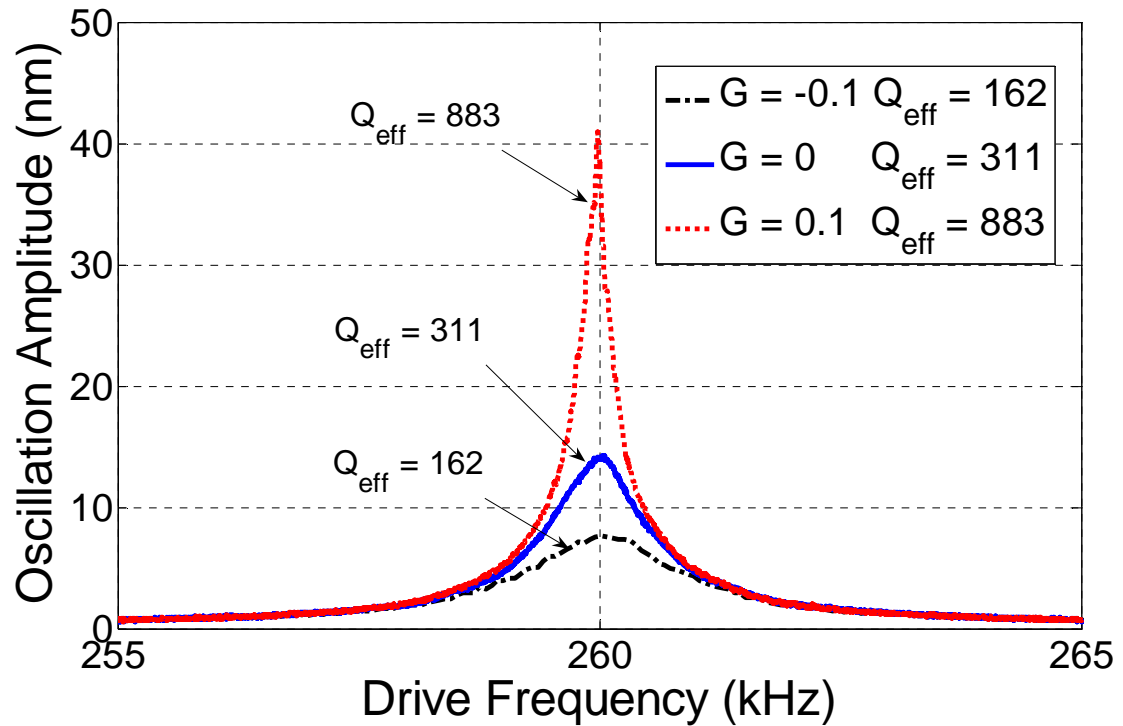


Figure 3.1: The amplitude response of the cantilever around the resonance frequency for different values of effective quality factor is obtained through experimental measurements.

3.2 Force Interactions

The force interactions between the probe tip and sample geometry is modeled as a spherical object interacting with a flat surface [19-21]. In the tapping mode AFM, the cantilever is oscillated over the sample surface and contacts the surface for a brief period of time at each oscillation cycle. As a result, the distance h between the cantilever tip and sample surface

changes continuously. Depending on the separation distance, two different interaction models are typically utilized to calculate the tip-sample forces.

3.2.1 Non-contact Forces

: For the separation distances larger than the inter-atomic distance a_0 , the long range attractive force is dominant (note that electro-static interactions are ignored). The attraction results from the integration of van der Waals energy between two atoms over the atoms of interacting surfaces. The van der Waals attraction force between a sphere and a flat surface is the negative gradient of this energy and can be written as a function of tip-sample separation distance h , the tip radius R , and the Hamaker constant H as follows [22]

$$F_{\text{vdw}}(h) = \frac{HR}{6h^2} \quad \text{if } h > a_0. \quad (3.3)$$

3.2.2 Contact Forces

It is assumed that a mechanical contact between the cantilever tip and the sample surface occurs when the separation distance h is smaller than the inter-atomic distance a_0 (negative values of h indicate indentation into the sample surface). During the contact, both adhesive and repulsive forces are effective. According to the DMT theory [23], the adhesion force is equal to the van der Waals attraction force when $h = a_0$. The repulsive force arising from

the mechanical contact of the tip with the sample surface is modeled using contact mechanics. Hence, the total force acting on the cantilever tip due the adhesive and repulsive components is given by

$$F_{\text{contact}}(h) = -\frac{HR}{6a_0^2} + \frac{4}{3}E^*\sqrt{R}(a_0 - h)^{3/2} \quad \text{if } h < a_0.$$

$$\frac{1}{E^*} = \frac{(1 - \nu_t)^2}{E_t} + \frac{(1 - \nu_s)^2}{E_s} \quad (3.4)$$

where E^* is the effective Young's modulus of the tip-sample pair, E_t and E_s are the elastic moduli of the tip and surface materials, ν_t and ν_s are the Poisson's ratio of the tip and the surface material, respectively.

Combining the contact and non-contact forces, the interaction force F_{ts} between the tip and the surface can be expressed as:

$$F_{ts}(h) = \begin{cases} -\frac{HR}{6h^2} & \text{if } h > a_0 \\ -\frac{HR}{6a_0^2} + \frac{4}{3}E^*\sqrt{R}(a_0 - h)^{3/2} & \text{else} \end{cases} \quad (3.5)$$

Chapter 4

SIMULINK MODEL

Simulating the dynamical behavior of the cantilever alone does not help us to investigate the scan performance under Q control for different scan settings. We also developed the models of the individual scan components and then integrated them with the model of the cantilever using SIMULINK to perform end-to-end scanning simulations.

4.1. Models of the Physical Components in the Setup

In addition to the force and the cantilever models described in the previous section, the complete SIMULINK model of the scanning system (shown in Figure 4.1.b) also includes the numerical models of the following physical components:

4.1.1 Vibrometer: The Laser Doppler Vibrometer (LDV) in the physical set-up is modeled as a block which differentiates the vibration signal (i.e. AC deflection of the cantilever) first and then outputs it after adding a time-delay on it. This time-delay is caused by the

digital signal processing unit of the LDV and confirmed to be fixed for the operating frequency of the cantilever [13].

4.1.2 RMS Converter: This block is used to compute the RMS of the vibration velocity. A built-in SIMULINK block (RMS in SimPowerMechanics Library) is used for this operation and the RMS value of the input signal is calculated over a running window. In order to calculate the oscillation amplitude of the cantilever, the RMS of the velocity signal is multiplied by a proper gain K as shown in Figure 4.1.b.

4.1.3 PI Scan Controller: This block is used to control the vertical movements of the computer-controlled XYZ stage. It has an analog to digital converter that samples the error signal at a fixed sampling rate. A built-in block of SIMULINK (*pid* controller) is utilized to actuate the XYZ stage based on the error in the peak-to-peak amplitude of the cantilever oscillations ($A_{\text{set}} - A$).

4.1.4 XYZ Stage: In order to model the dynamics of the computer controlled XYZ nano stage used in the physical set-up, we have used a first order transfer function with a time constant smaller than the sampling time of the PI controller. The vertical movements of the XYZ stage are represented as s_2 in Figure 4.1.

4.1.5 Adaptive Q Controller: This block is used to calculate the gain $G(t)$ which depends on the peak-to-peak oscillation amplitude of the cantilever. If $G(t)$ is set to a constant value, this block functions as a standard Q controller. In AQC, the gain is adjusted on the fly depending on the RMS value. The output of this block, $G(t)$ is used to scale the velocity signal first and then the scaled signal (F_{AQC}) is added on the drive signal in order to change the Q_{eff} of the cantilever.

4.2. Models for Input/Output Operations

In addition to the models of above components, the following blocks are used for regulating input-output operations:

4.2.1 Input Profile: This block generates the input surface profile as a function of time. In the case of scanning calibration steps with a constant height of h_s and width of w_s , the input profile s_1 is periodic with a period of $t_s = w_s / v_s$, where v_s is the scan speed. For the time interval $0 < t < t_s$, s_1 is given by

$$s_1 = \begin{cases} 0 & 0 < t < \frac{t_s}{2} \\ h_s & \frac{t_s}{2} < t < t_s \end{cases} \quad (4.1)$$

4.2.2 Output Profile: This is the block where the inverse of the movements of the XYZ stage (s_2) are recorded. Hence, this is the output of the scanning system. The output scan profile should exactly match the desired input profile (s_1) under ideal conditions.

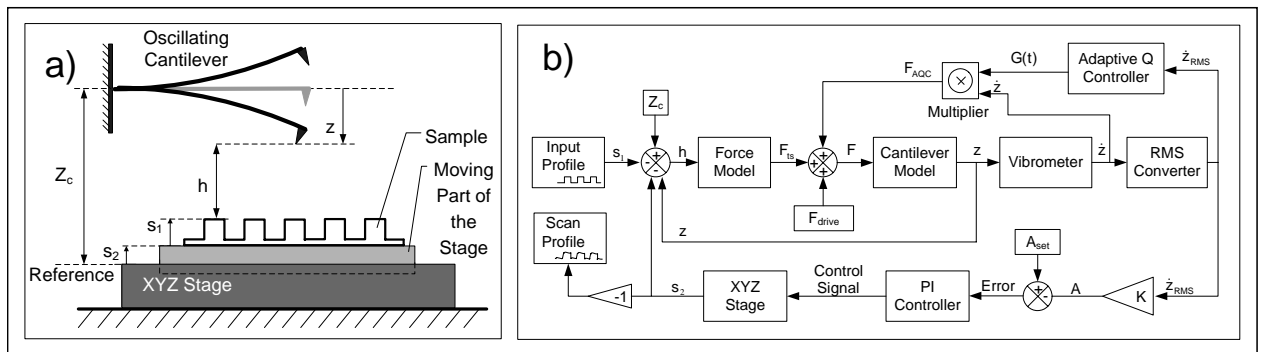


Figure 4.1: SIMULINK model of our experimental scanning set-up.

In the SIMULINK model, the parameters Z_c , h , and z represent the vertical position of the resting cantilever with respect to the reference plane in the absence of tip-sample interaction, the vertical separation distance between the cantilever tip and the sample surface, and the instantaneous vertical position of the oscillating cantilever with respect to its resting position, respectively (Figure 4.1.a).

Chapter 5

SCANNING SIMULATIONS and EXPERIMENTS

In this section, we investigate standard Q control and then extend our work to show the benefits of using AQC through numerical simulations performed in SIMULINK and also by conducting scanning experiments with our physical AFM set-up. In standard Q control, the gain G is set to a constant value prior to scanning in order to increase or decrease the Q_{eff} of the cantilever and is not altered during scanning. In AQC, the Q_{eff} of the cantilever is adjusted in real time depending on the surface profile by setting the gain G adaptively.

We first investigate the effect of Q factor and stiffness of a cantilever probe on its sensitivity in scanning soft and stiff samples through numerical simulations. For this purpose, we performed scanning simulations with a 10 nm height soft sample ($E_{\text{sample}} = 200$ MPa) lying on a stiffer substrate ($E_{\text{substrate}} = 10$ GPa). This is a typical scenario encountered when scanning soft samples in liquid where the Q factor of the cantilever is significantly reduced due to the environmental damping. The simulations are repeated for cantilevers with Q_{eff} ranging from 10 to 800 and three different stiffness constants for $k = 0.05$ N/m, 0.5 N/m, and 5 N/m. All other parameters in the SIMULINK model, such as the PI

controller gains, the material properties of the cantilever tip, scan speed, resonance frequency and free-air amplitude of the cantilever, are kept constant throughout the simulations. As shown in Fig. 5.1.a, the apparent (measured) height of the scanned sample depends on Q_{eff} and cantilever stiffness. As Q_{eff} is increased and k is decreased, the apparent height approaches to the actual value. Our numerical simulations show that scanning in attractive regime using soft cantilevers with high Q_{eff} results in a better image quality. The sudden jumps to the actual value shown in Figure 5.1.a for $k = 0.05 \text{ N/m}$ and 0.5 N/m occurs when the cantilever starts to operate at the attractive regime. In this regime, non-contact forces are effective only. The probe is not tapping on the sample surface and oscillation amplitude is reduced only by the non-contact interactions [21]. Since the probe tip is not in physical contact with the sample surface during this period, there is no sample deformation and hence no difference between the measured and actual heights of the sample.

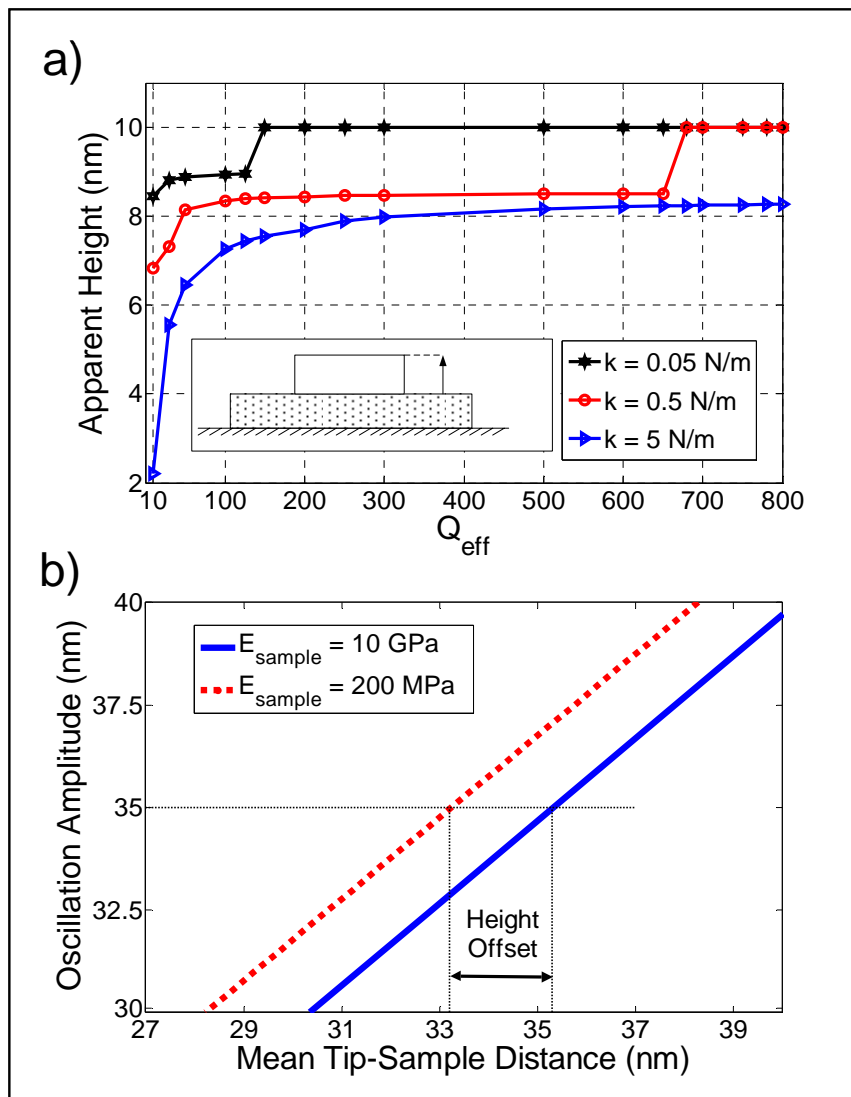


Figure 5.1: a) Apparent height of a 10 nm sample ($E_{\text{sample}} = 200$ MPa) lying on a stiffer substrate ($E_{\text{substrate}} = 10$ GPa) for different values of effective quality factor and stiffness constant of the cantilever. b) Oscillation amplitude versus mean tip-sample distance for samples having different elastic modulus ($A_{\text{set}} = 35$ nm, $A_0 = 50$ nm).

If the scanning is performed in the repulsive regime, where the cantilever tip touches the sample surface, the offset between the measured and actual heights is more prominent, especially for stiffer cantilevers. In this regime, the contact mechanics dominates the interactions between the probe tip and the sample surface. Hence, the elastic moduli of the cantilever tip and sample surface both influence the scan quality. In Figure 5.1.b, we show the change in the oscillation amplitude of a cantilever probe as a function of the tip-sample distance when the probe tip interacts with soft ($E_{\text{sample}} = 200 \text{ MPa}$) and stiff samples ($E_{\text{sample}} = 10 \text{ GPa}$) lying on a stiff substrate ($E_{\text{substrate}} = 10 \text{ GPa}$). The cantilever tip indents more into the soft sample than it does into the stiffer one to reach the same set amplitude and hence a height offset in the order of nanometers occurs when scanning soft samples. From the numerical simulations, we observe that this problem is more pronounced if the Q_{eff} of the cantilever is low, as it occurs when the probe is immersed into liquid. These numerical simulations show a good agreement with the experimental studies of Ebeling et al. [24] and Humphris et al. [5]. In both of those studies, an increase in the apparent height of DNA on mica is reported when the effective quality factor of the cantilever is enhanced. In the case of scanning samples as stiff as the substrate surface, the height offset becomes insignificant. Although the scanning is performed in repulsive regime, the indentation of the probe tip into the sample surface is minimal throughout the sample surface independent of the cantilever stiffness.

Secondly, we consider the effect of Q factor on the tapping forces. In addition to the material properties of the sample, the force interactions between the probe tip and the sample surface also depend on the free-air oscillation amplitude A_0 and the set amplitude A_{set} of the probe when scanning under Q control. We performed numerical simulations to investigate the effect of A_{set} (as a percentage of A_0) and Q_{eff} on the tapping forces. In Figure 5.2.a, we present the magnitude of maximum tapping force as a function of A_{set}/A_0 for different values of Q_{eff} . The maximum tapping force is calculated based on the average of maximum indentations of the probe tip into the sample surface after the tapping amplitude reaches to steady state (i.e. $A = A_{\text{set}}$). As A_{set}/A_0 approaches to one, the probe tip starts tapping the sample surface lightly and the resultant interaction forces decrease. Similarly, as Q_{eff} increases, the tapping forces also decrease. However, for a given A_{set}/A_0 , the rate of decrease in tapping forces is less significant as Q_{eff} increases (Figure 5.2.b). For scanning soft samples in liquid, keeping the tapping forces low is crucial in order to prevent damaging the sample. It is also desired to have lower tapping forces to prevent the tip wear during the scanning of stiffer surfaces in air as well.

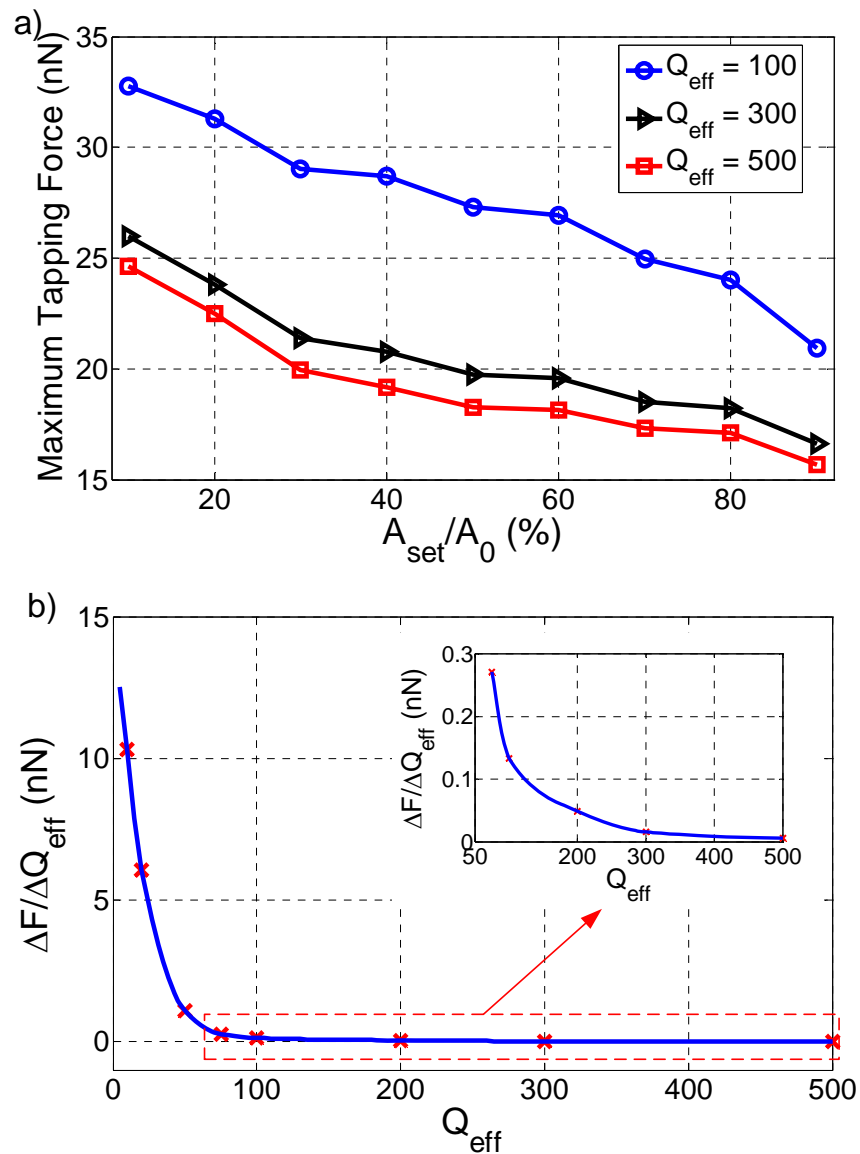


Figure 5.2: a) Maximum tapping forces as a function of effective quality factor for different set amplitudes. b) The rate of change in tapping forces as a function of effective quality factor for $A_{\text{set}}/A_0 = 70\%$.

Increasing the Q factor, especially when operating in liquid, has the benefits of decreasing the tapping forces and improving the sensitivity of probe such that soft samples can be traced better. However, if the sample surface is stiffer and the native Q factor of the cantilever probe is already high, which is typically the case when scanning in air, the probe sensitivity has a limited influence, but its slow transient response adversely affect the image quality. The bandwidth of the cantilever that is how fast it responds to the changes in surface profile is inversely proportional to its Q factor. As a result, increasing the Q factor limits the maximum achievable scan speed [11, 12]. In order to show the effect of Q factor of a cantilever on its bandwidth and in return to the maximum achievable scan speed, we present the simulation results of scanning a 100 nm step for three different values of $Q_{\text{eff}} = 10, 400, \text{ and } 1000$ (see Figure 5.3). As the Q_{eff} is increased, the response of the probe to the rapid changes in surface profile becomes slower and it cannot trace the input profile well. As shown in Figure 5.3, it takes longer time for the cantilever to return to the set amplitude when a downward step is encountered.

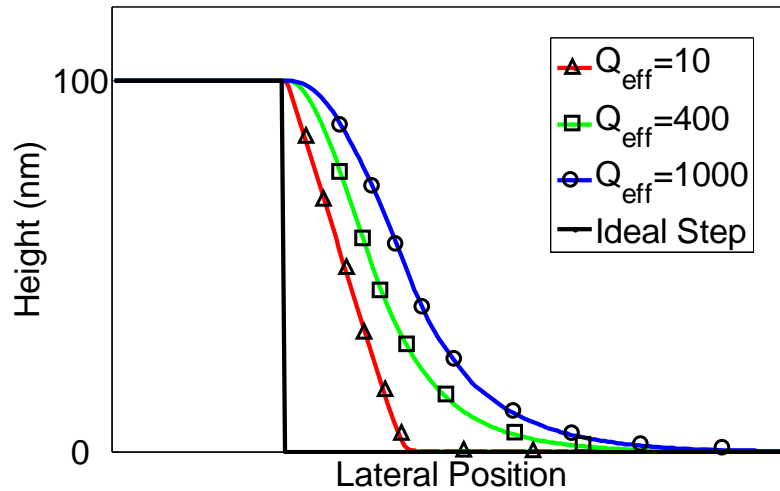


Figure 5.3: Scanning a downward step using a cantilever having different values of effective quality factor.

Therefore, there is a trade-off between the maximum achievable scan speed and the tapping forces applied to the sample when scanning under Q control. Higher Q values promote lower tapping forces while lower ones result in an increased scanning speed. In order to show this trade-off more quantitatively, we performed simulations of scanning in tapping mode AFM for different values of A_{set} and scan speeds. We have defined an error measure to evaluate and compare the scan performances under different scan settings. This measure is based on the positional error between the measured (output) and desired (input) scan profiles. We first define e_x as the absolute value of the positional difference between the measured and actual heights of the sample surface at a lateral position x along a scan line.

Then, the total scan error, e_s , is calculated by integrating the positional error e_x over the scan-line. The magnitude of the scan error is zero if the resultant scan profile is exactly matches the actual surface profile. In the case of scanning calibration steps with a constant height of h_s (see Figure 5.4), the total scan error is calculated by first integrating the positional error e_x over a full step width w_s and then normalizing the sum by the area under the step. This normalization makes the scan error invariant of the scan speed so that it can be used for comparing the results of different scan speeds. Hence, the scan error e_s is calculated as

$$e_s = \frac{\int_0^{w_s} |e_x| dx}{w_s h_s} \quad (5.1.)$$

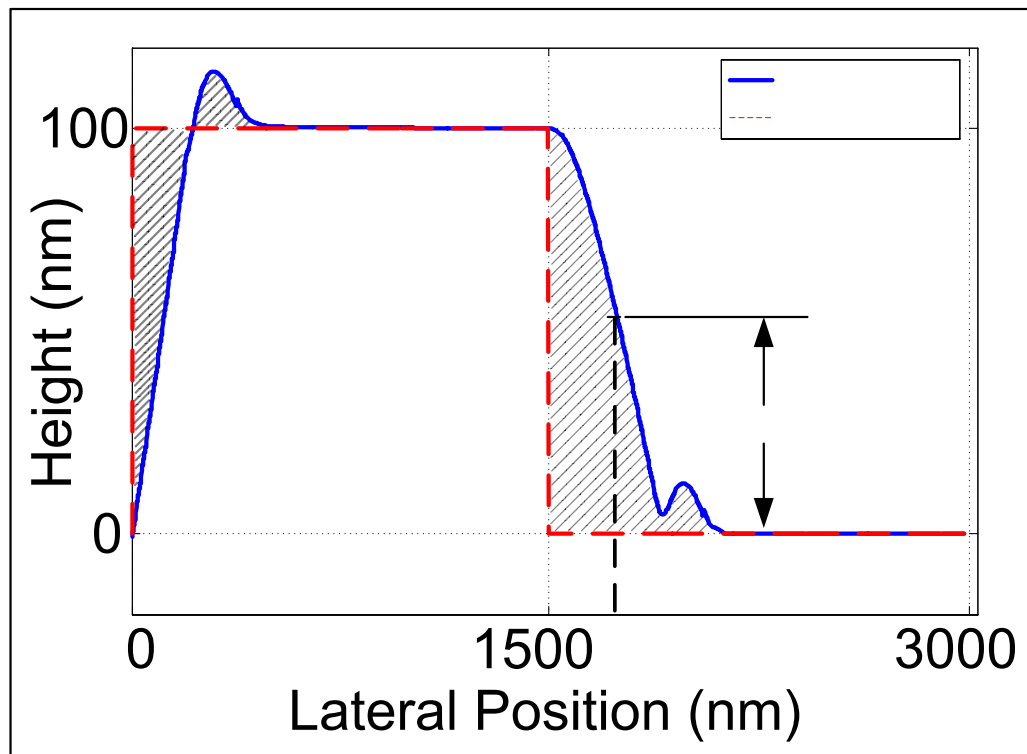
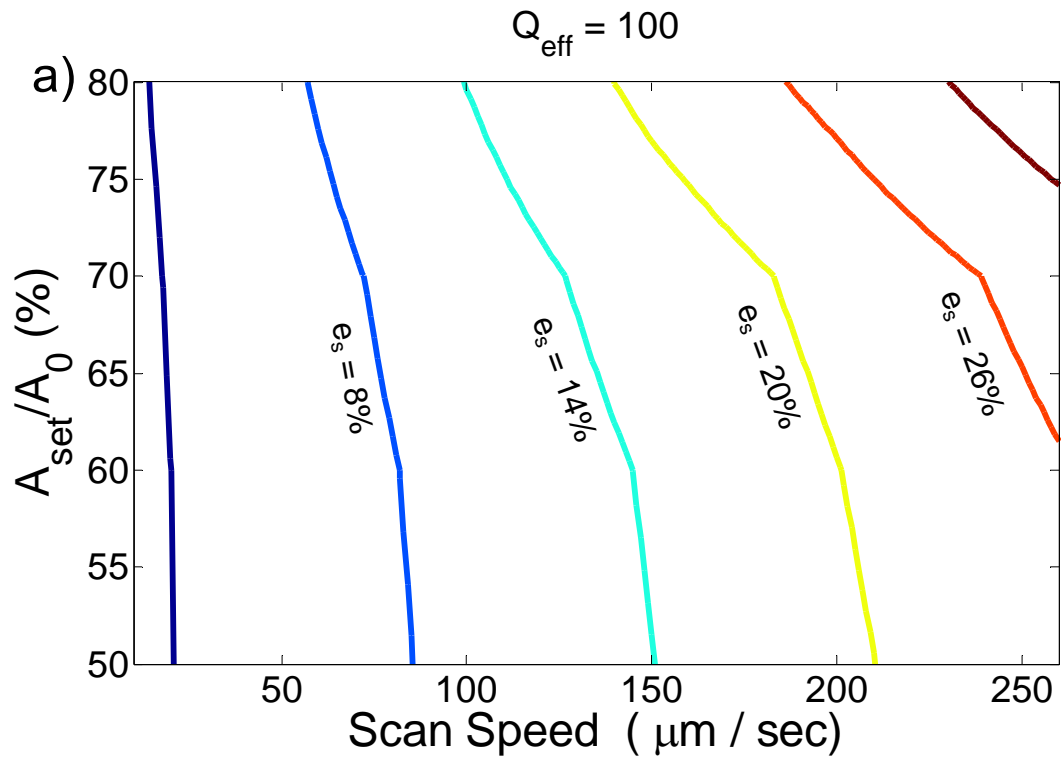


Figure 5.4: Scan profile (blue solid line) of an ideal step (red dashed line) with a height of $h_s = 100$ nm and width of $w_s = 3$ μm .

In Figure 5.5, we present the iso-error curves obtained by scanning a 100 nm step under Q control for $Q_{\text{eff}} = 100$ and 500. It is observed that the scan error increases as the scan speed and A_{set} increase. Also, increasing the Q factor of the cantilever causes higher scan errors. However, recall that tapping forces are reduced as the Q factor is increased (see Figure 5.2.a). The influence of A_{set} on this trade-off becomes more prominent when operating at

higher scan speeds (iso-error lines become more inclined as move to the right on the speed axis in Figure 5.5).



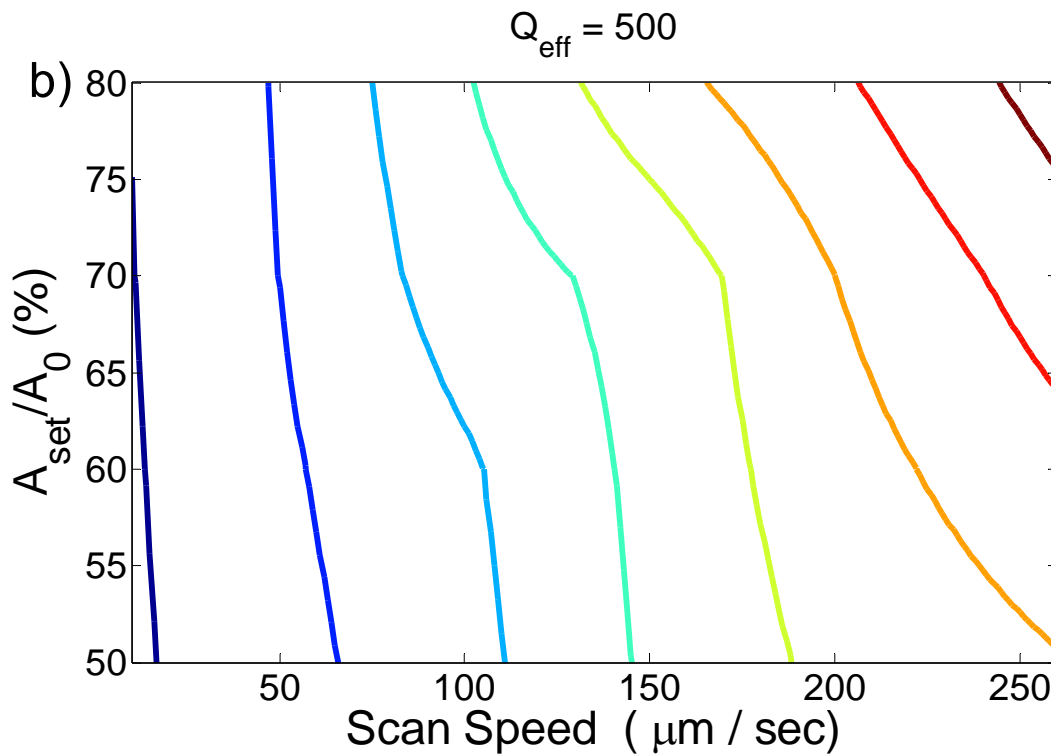
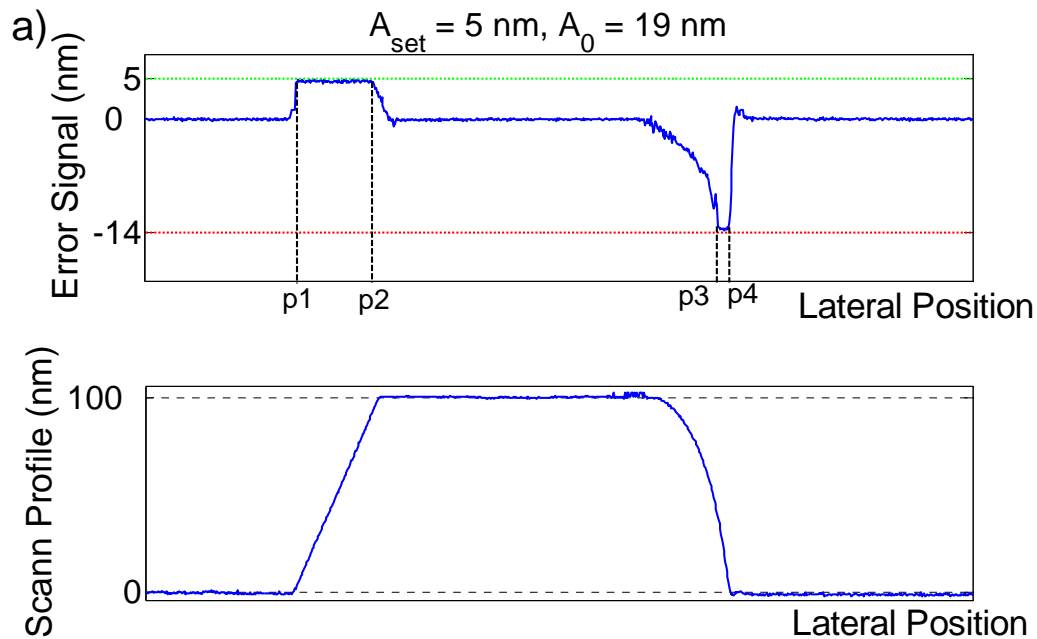


Figure 5.5: Iso-error curves for the scan results of a 100 nm step for $Q_{\text{eff}} = 100$ (a) and $Q_{\text{eff}} = 500$ (b).

While the tapping forces are reduced as Q factor is increased, the transient response of the probe becomes slower and hence the error signal saturates for a longer period of time, limiting the maximum achievable speed. For example, when scanning steps with a constant height, the error saturation occurs at the beginning and end of the step. When an upward step is encountered, the probe tip suddenly sticks to the surface, the oscillation amplitude reduces to zero and the error signal ($A_{\text{set}} - A$) saturates at A_{set} (see the error signal between

the lateral positions $p1$ and $p2$ in Figure 5.6). When a sharp downward step is encountered, the oscillation amplitude of the probe reaches to its free air value and the error signal this time saturates at $A_{\text{set}} - A_0$ (see the error signal between the lateral positions $p3$ and $p4$ in Figure 5.6). Choosing a high value for A_{set} reduces the saturation problem at the beginning of the step (since the magnitude of the error signal is high, the controller responds more rapidly) and also reduces the tapping forces (see Figure 5.2.a), but amplifies the saturation problem at the end of the step. These saturations result in an inclined profile at the entrance and exit of the step (see scan profiles in Figure 5.6).



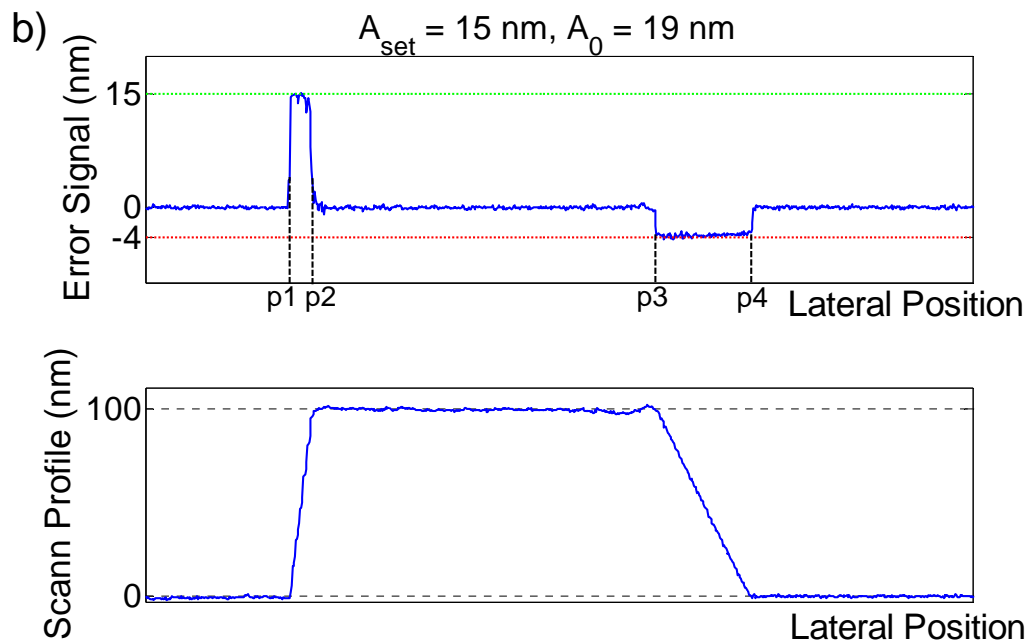


Figure 5.6: The error saturations when $A_{\text{set}} = 5 \text{ nm}$ (a) and 15 nm (b) $A_0 = 19 \text{ nm}$. The lateral positions where the error saturation occurs are marked as “p1”, “p2”, “p3”, and “p4” on the figures.

The error saturation is also adversely affected by the increase in scan speed. This, in fact, limits the maximum achievable scan speed. In Figure 5.7.a and Figure 5.7.c we present the experimental results scanning 100 nm calibration steps using conventional PI scan controller for two different scan speeds of $2 \mu\text{m}/\text{sec}$ and $10 \mu\text{m}/\text{sec}$, respectively. The other scan parameters are kept constant during the experiments and hence the elapsed time during error saturations are the same at both scan speeds. However, the lateral distance traveled during the error saturated period is different, resulting in a less accurate scan

profile for the faster scan (and Figure 5.7.c). Hence, the error saturation is a major problem limiting the maximum achievable scan speed when scanning samples having sharp changes in topography. The same scanning experiments are simulated using SIMULINK and the results are presented in Figure 5.7.b and Figure 5.7.d. The scan parameters used in simulations are matched to the ones used in the physical experiments. The resultant scan profiles obtained through numerical simulations show a good agreement with the experimental ones and the saturation problem is also observed.

The AQC reduces the error saturation problem leading to an increase in scan speeds with no increase in tapping forces (Figure 5.7.e). As an alternative, the integral gain constant of the PI controller can be increased to overcome the saturation problem [25]. However, there is an upper limit for its value. A higher controller gain magnifies the noise in the measurement (i.e. cantilever deflection signal) and significantly reduces the quality of the resultant image.

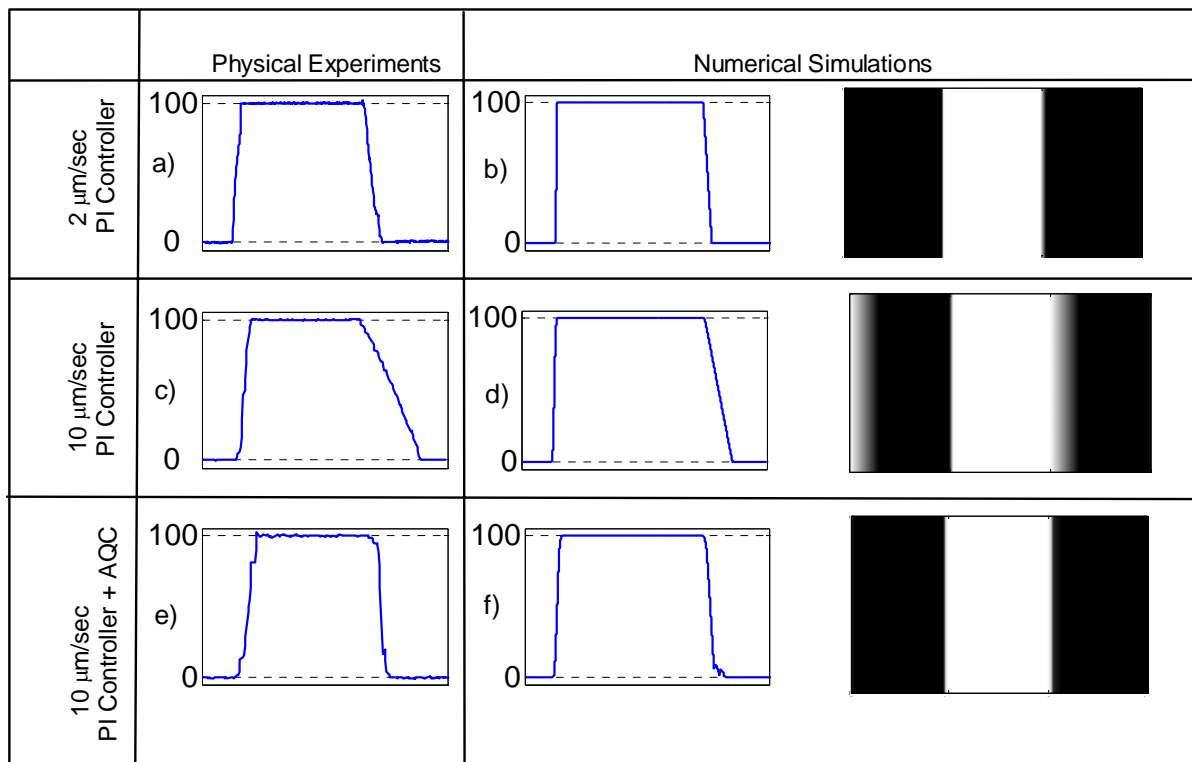


Figure 5.7: Results of the experimental and numerical scans with and without AQC for the scan speeds of 2 $\mu\text{m}/\text{sec}$ and 10 $\mu\text{m}/\text{sec}$.

As can be seen from the figure, the cantilever probe tracks the input profile better in AQC, resulting in a sharper image. In AQC, the Q factor of the probe is set to an initial value as in standard Q control, but then modified on the fly during scanning when necessary. For example, if the error saturation is detected when scanning a downward step, AQC automatically increases the gain G (and hence the Q factor of the probe). This saturation occurs when $A > A_{\text{threshold}}$, where $A_{\text{threshold}}$ is a threshold value close A_0 . An increase in the

Q factor causes an increase in the vibration amplitude A as well as the magnitude of the error signal (Figure 5.8), which results in a faster response of the z-actuator moving the sample. As a result, the adverse effects of the error saturation on the output profile are significantly reduced using AQC. Moreover, since the free-air saturation problem is suppressed using AQC, one can use a higher A_{set} to reduce the tapping forces as well as the error saturation at the beginning of the step as discussed earlier.

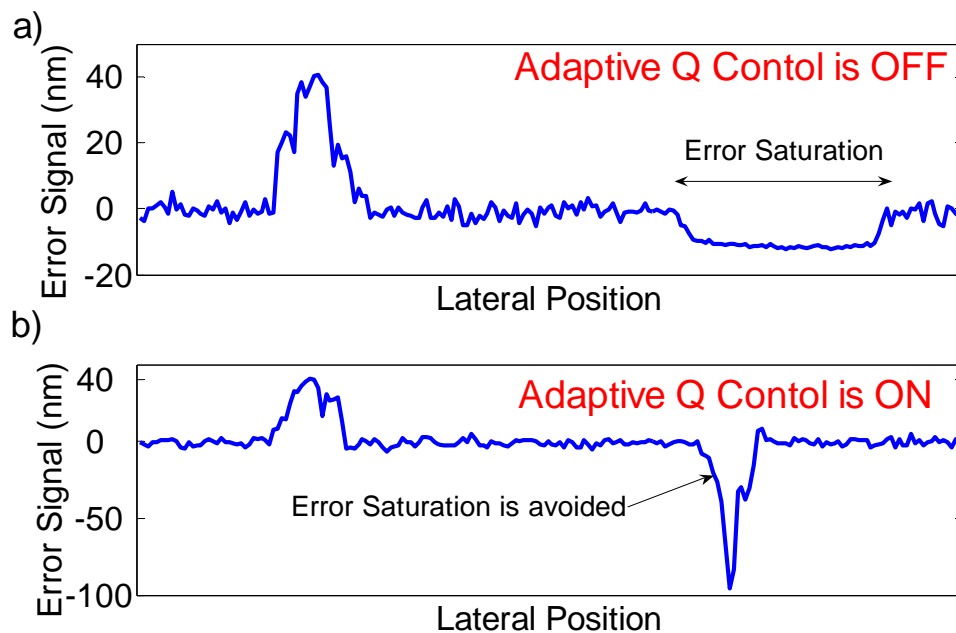


Figure 5.8: The error signal during the scanning of 100 nm calibration steps (scan speed = 10 $\mu\text{m}/\text{sec}$) when the adaptive Q controller is turned off (a) and on (b). The error saturation observed in (a) is avoided using AQC (b).

In Figure 5.9, we compare the performance of standard Q control and AQC using iso-error lines obtained by numerical simulation of scanning 100 nm steps. For a scan error of $e_s = 20\%$ and $A_{\text{set}}/A_0 = 70\%$, one can easily reach higher scan speeds using AQC for $Q_{\text{eff}} = 300$. However, the Q factor of the probe must be reduced to $Q_{\text{eff}} = 5$ in standard Q control to achieve the same speed for exactly the same error level, but this causes an increase of approximately nine folds in tapping forces.

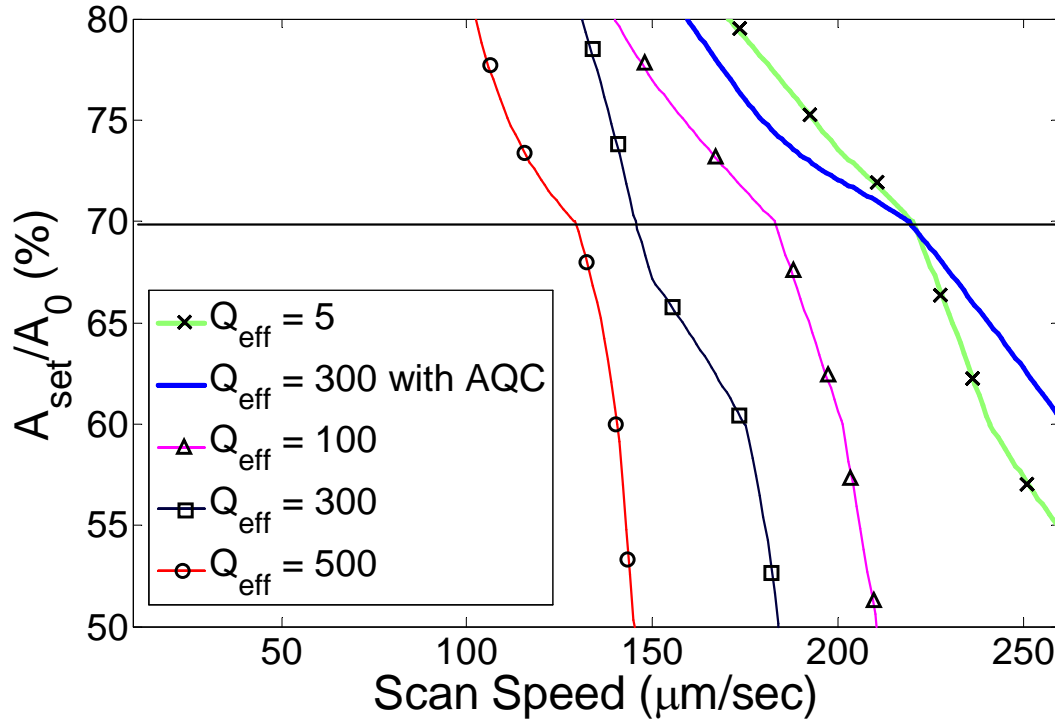


Figure 5.9: Comparison of standard Q control and AQC using iso-error curves for the scan error of $e_s = 20\%$.

Chapter 6

DISCUSSION AND CONCLUSION

The trade off in setting the Q factor of a cantilever probe in standard Q control was numerically analyzed and its performance in scanning nano surfaces was quantitatively compared to that of AQC using an error measure. The results of the numerical simulations were validated through scan experiments performed in a physical set-up. Although numerical simulations have been performed in the past to investigate cantilever dynamics and tip-sample interactions, only a few recent studies have focused on the simulation of whole scan process [14]. Without numerical scanning simulations, it is highly challenging to repeat a scan experiment in a physical setting under the same exact conditions (e.g. humidity, electrical noise, ground vibrations, temperature, etc). Even if we provide the same physical conditions, the probe tip or the sample surface may be damaged in time, which affects the scan results adversely. All these factors make it impossible to compare the results of experimental scans for different settings in real world. On the other hand, through numerical simulations, we constructed performance lines of constant error for different scan parameters and controllers. Using these iso-error lines, we quantitatively compared the performance of standard Q control with AQC. In addition, it is possible to

access the scan outputs in numerical simulations that are not directly measurable during physical experiments such as the magnitude of tapping forces or indentation amplitudes (Figure 5.2). Moreover, one can also run “what-if” scenarios in a simulation world to investigate the scan performance in different environment such as liquid or air. For example, we investigated the effect of stiffness constant and Q factor of a cantilever on the resultant scan profile when scanning a soft object in liquid (Figure 5.1). We showed that scanning in attractive regime using soft cantilevers having high Q_{eff} results in a better image quality. If a soft sample is scanned in such an environment where the Q factor drops significantly, the probe tip cannot accurately trace the surface profile and the size of the sample is typically measured less than its actual value. Moreover, there is a risk of damaging the soft sample due to high tapping forces at low Q factor (Figure 5.2.a). To overcome these problems, the Q factor of the cantilever is increased using standard Q control when scanning in liquid. On the other hand, when scanning in air, the native Q factor of the cantilever is already high and increasing it further does not significantly reduce the tapping forces. Our simulation results show that the magnitude of tapping forces is high at low Q_{eff} and decreases as the Q_{eff} is increased while the rate of drop is not significant at higher values (see Figure 5.2.b). Moreover, the slow transient response of the cantilever at high values of Q_{eff} limits the maximum achievable scan speed. Hence, reducing the Q factor increases the scan speed, but it also increases the magnitude of tapping forces, which may cause damage to the cantilever probe tip and sample. As shown

in Figure 5.9, it is possible to achieve higher scan speeds using AQC without causing an increase in the tapping forces. We showed that error saturation is a major factor limiting the scan speed in tapping mode and AQC solves this problem (see Figure 5.8). In AQC, if there is a tendency towards saturation in error signal (due to the rapid variations in surface topography), the controller changes the Q factor of the probe instantaneously to avoid the saturation problem. Moreover, since the error saturation problem is suppressed using AQC, one can use higher values of A_{set} to reduce the tapping forces (see the relation in Figure 5.2.a).

BIBLIOGRAPHY

- [1] Zhong Q., Imniss D., Kjoller K., Elings V.B., Fractured polymer/silica fiber surface studied by tapping-mode atomic force microscopy, *Surface Science*, 290, (1993), 688-692.
- [2] Anczykowski B., Cleveland J.P., Krüger D., Elings V., Fuchs H., Analysis of the interaction mechanisms in dynamic mode SFM by means of experimental data and computer simulation, *Applied Physics A: Materials Science Processing*, 66, (1998), 885.
- [3] Tamayo J., Humphris A.D.L., Owen R.J., Miles M.J., High-Q dynamic force microscopy in liquid and its application to living cells, *Biophysical Journal*, 81, (2001), 526.
- [4] Grant A. and McDonnell, L., A non-contact mode scanning force microscope optimized to image biological samples in liquid, *Ultramicroscopy* 97, (2003), 177
- [5] Humphris A. D. L., Round A. N. and Miles M. J., Enhanced imaging of DNA via active quality factor control, *Surf. Sci.* 491, (2001), 468.
- [6] Rodriguez T.R., Garcia R., Theory of Q control in atomic force microscopy, *Applied Physics Letters*, 82, (2003), 4821.
- [7] Kokavecz J., Horvath Z.L., Mechler A., Dynamical properties of the Q-controlled atomic force microscope, *Applied Physics Letters*, 85, (2004), 3232.
- [8] Hoscher H., Ebeling D. and Schwarz U. D., Theory of Q-Controlled dynamic force microscopy in air, *J. Appl. Phys.* **99**, (2006), 084311.
- [9] Jäggi R. D., Franco-Obregón A., Studerus P. and Ensslin K., Detailed analysis of forces influencing lateral resolution for Q-Control and tapping mode, *Appl. Phys. Lett.*, 79, (2001), 135.
- [10] San Paulo A., Garcia R., Unifying theory of tapping-mode atomic force microscopy, *Physical Review B*, 66, (2002), 041406.

-
- [11] Sulchek, T., Hsieh R., Adams J. D., Yaralioglu G. G., Minne S. C., Quate C. F., Cleveland J. P., Atalar A., and Adderton D. M., High-speed tapping mode imaging with active Q control for atomic force microscopy, *Appl. Phys. Lett.*, 76, (2000), 1473.
- [12] Sulchek, T., Yaralioglu, G. G., Quate, C. F., Minne, S. C. , Characterization and optimization of scan speed for tapping-mode atomic force microscopy, *Review of Scientific Instruments*, 73 (8), (2002), 2928-2936.
- [13] Gunev I., Varol A., Karaman S. and Basdogan C., Adaptive Q control for tapping-mode nanoscanning using a piezoactuated bimorph probe, *Rev. Sci. Instrum* **78**, 4 (2007)
- [14] Kowalewski T. and Legleiter J., Imaging stability and average tip-sample force in tapping mode atomic force microscopy, *J. Appl. Phys.*,99 (2006) 064903
- [15] Veeco Instruments, Probes Catalog (2006).
- [16] Garcia R., Pérez R., *Dynamic Atomic Force Microscopy Methods*, *Surface Science Reports*, 47, (2002), 197-301.
- [17] Schitter G., Menold P., Knapp H. F., Allgöwer F. and Stemmer A., High performance feedback for fast scanning atomic force microscopes, *Rev. Sci. Instrum.*, 72(8), (2001), 3320-3327.
- [18] San Paulo A. and García R., Tip-surface forces, amplitude, and energy dissipation in amplitude-modulation (tapping mode) force microscopy, *Phys. Rev. B* 64, (2001), 193411.
- [19] Perez R., Stich I., Payne M. C. and Terakura K., Surface-tip interactions in noncontact atomic-force microscopy on reactive surfaces: Si(111), *Phys. Rev. B*, 58 (16), (1998), 10835-10849.
- [20] García R. and San Paulo A., Attractive and repulsive tip-sample interaction regimes in tapping-mode atomic force microscopy, *Phys. Rev. B*. **60**, 4961, (1999).
- [21] Aimé J. P., Boisgard R., Nony L., and Couturier G., Nonlinear Dynamic Behavior of an Oscillating Tip-Microlever System and Contrast at the Atomic Scale, *Phys. Rev. Lett.* 82, (1999), 3388.

- [22] Israelachvili J., *Intermolecular and Surface Forces* (Academic, London, 1995).
- [23] Derjagurin B.V., Muller V.M., Toporov Y.P., Effects of contact deformations on the adhesion of particles, *Journal of Colloid Science*, 53, (1975), 314.
- [24] Ebeling D., Hölscher H., Fuchs H., Anczykowski B., Schwarz U.D., Imaging of biomaterials in liquids: a comparison between conventional and Q-controlled amplitude modulation ('tapping mode') atomic force microscopy, *Nanotechnology*, 17, (2006), S221.
- [25] Kodera N., Sakashita M., Ando T., Dynamic proportional-integral-differential controller for high-speed atomic force microscopy, *Review of Scientific Instruments*, 77, (2006)

VITA

Aydın Varol was born in Istanbul, Turkey, on October 13, 1983. He graduated from Gaziantep Fen Lisesi in 2000. He received his BS degree in Mechanical Engineering and Computer Engineering from Koc University, Istanbul in 2005. Same year, he joined the M.S. program in Mechanical Engineering at Koc University as a research and teaching assistant. Next year, he will be a Ph.D. candidate in Computer Science at Ecole Polytechnique Fédérale de Lausanne, Switzerland.